

Incrementally Stochastic and Accelerated Gradient Information mixed Optimization for Manipulator Motion Planning

Feng Yichang, Zhang Haiyun, Wang Jin*, Lu Guodong

Abstract—This paper introduces a novel motion planning algorithm, incrementally stochastic and accelerated gradient information mixed optimization (iSAGO), for robotic manipulators in a narrow workspace. Primarily, we propose the overall scheme of iSAGO integrating the accelerated and stochastic gradient information for efficient descent in the penalty method. In the stochastic part, we generate the adaptive stochastic moment via the random selection of collision checkboxes, interval time-series, and penalty factor based on Adam to solve the body-obstacle stuck case. Due to the slow convergence of STOMA, we integrate the accelerated gradient and stimulate the descent rate in a Lipschitz constant reestimation framework. Moreover, we introduce the Bayesian tree inference (BTI) method, transforming the whole trajectory optimization (SAGO) into an incremental sub-trajectory optimization (iSAGO) to improve the computational efficiency and success rate. Finally, we demonstrate the key coefficient tuning, benchmark iSAGO against other planners (CHOMP, GPMP2, TrajOpt, STOMP, and RRT-Connect), and implement iSAGO on AUBO-i5 in a storage shelf. The result shows the highest success rate and moderate solving efficiency of iSAGO.

I. INTRODUCTION

The industrial robot has been widely applied in various areas such as welding and products loading or placing. The industrial robot always executes the above tasks under manual teaching or programming. So automatic production urges an efficient and robust optimal motion planning (OMP) algorithm to elevate industrial intelligence. Many former OMP studies gain a collision-free optimal trajectory via numerical optimization or probabilistic sampling.

The main concern of numerical optimization is how to descend to an optimum rapidly. CHOMP [1] and GPMP [2] adopt the gradient descent method with the fixed step size. CHOMP uses HMC [3] for success rate improvement. To lower the computational cost, GPMP and dGPMP [4] adopt iSAM2 [5] and do an incremental OMP (iOMP) via LM [6] method. Moreover, TrajOpt [7] uses trust-region [8] method to expedite the OMP process. Nevertheless, the above methods could guide the trajectory into the local minima informed by gradient. Accelerated gradient descent (AGD) [9], [10] has recently been developed and implemented in optimal control [11], [12] of a dynamic system described by differential equations whenever the objective is strongly convex. Moreover, stochastic optimization (SO) employs the momentum theorems of AGD and solves the large-scale semi-convex cases [13], which generates stochastic sub-gradients via the

random sub-datasets selection. Adam [14] upgrades RM-SProp [15] and introduces an exponential moving average (EMA) based moment adaptation. Furthermore, [16] adopts it to assist UAVs to overcome an unknown disturbance.

Unlike the numerical methods, the sampling method finds an optimal trajectory via roadmap construction or trajectory sampling [17]. PRM [18], including its upgrade like PRM* [19] and RGGs [20]), makes a collision-free connection among the feasible vertexes to construct a roadmap. Then they construct an optimal trajectory via the all-pairs short paths (APSPs) methods, such as Dijkstra's algorithm [21] and Chehov [22], using a data structure storing and querying partial trajectories. Unlike PRM associated with APMPs, RRTs [23], including its upgrade like RRT* [19] and CODEs [24]) find a locally optimal trajectory via the growth of rapidly-exploring random trees.

Though the above methods could find a minimum rapidly or a feasible solution reliably via numerical optimization or probabilistic sampling, there remain two main contradictions: **1)** the numerical descent achieves a high computational efficiency though pays for **the low reliability (a.k.a. success rate)** because of the strong convexity requirement; **2)** the sampling method remedies the numerical limitation with probabilistic completeness regardless of the bulk of samples positively correlating to **the computational resource**.

In this way, this paper proposes SAGO integrating the exact and inexact stochastic information for OMP. **1) Stochastic trajectory optimization with moment adaptation (STOMA)** could overcome the local minimum mainly from the body-obstacle stuck case via the random variable selection, such as collision-check boxes (CCBs), time intervals, and penalty factors. However, the $\mathcal{O}(\log N/N)$ convergence rate of cost in STOMA means low computational efficiency. So, **2)** we propose **\mathcal{L} -restarted AGD (\mathcal{L} -reAGD)** in the non-stuck case with the gradient norm's $\mathcal{O}(1/N^{\frac{3}{2}})$ rate. **3)** SAGO adopts Bayesian tree inference (BTI) based iOMP and upgrades to **iSAGO**, elevating the efficiency further.

II. BACKGROUND

A. A Gauss-Markov model

The motion planning problem given the initial and goal states and environment information is a probabilistic inference. Its prior probabilistic model is formed by linear time-varying stochastic differential equation (LTV-SDE):

$$\dot{\theta}(t) = \mathbf{A}(t)\theta(t) + \mathbf{u}(t) + \mathbf{F}(t)\mathbf{w}(t), \quad (1)$$

where \mathbf{A} and \mathbf{F} are the matrices of the system and stochastic process, respectively, and $\mathbf{u}(t)$ is an input. The white noise

* Wang Jin, corresponding author, State Key Laboratory of Fluid Power and Mechatronic Systems, School of Mechanical Engineering, Zhejiang University, Hangzhou, Zhejiang, China. dwjcom@zju.edu.cn

process $\mathbf{w}(t)$ itself obeys a Gaussian distribution with zero-valued expectation and covariance matrix $\mathbf{Q}_c(t)\delta(t-t')$. [2] details how to estimate the mean $\boldsymbol{\mu}(t)$ and covariance $\mathbf{K}(t, t')$ of Gaussian process (GP) prior, generated by (1).

B. Objective functional

This paper adopts the objective functional proposed in CHOMP by [1] for the generation of an optimal trajectory in low energy cost without collision. In this way, we design the objective functional as:

$$\mathcal{F}[\boldsymbol{\theta}(t)] = \frac{\rho}{2} \|\boldsymbol{\theta} - \boldsymbol{\mu}\|_{\mathbf{K}}^2 + \int_{t_0}^{t_g} \int_{\mathcal{B}} c(\mathbf{x}) \|\dot{\mathbf{x}}\| du dt, \quad (2)$$

where λ is a trade-off parameter between the GP and obstacle functional, $c(\cdot) : \mathbb{R}^3 \rightarrow \mathbb{R}$ is a workspace cost function that penalizes a set of points $\mathcal{B} = \{\mathcal{B}_1, \dots, \mathcal{B}_{N_B}\} \subset \mathbb{R}^3$ on robot body when they are in or around an obstacle, $x(u)$ maps from robot configuration to workspace, and $\boldsymbol{\theta}, \mathbf{K}$ are the expectation value and covariance matrix of GP prior:

$$\boldsymbol{\theta}(t) \sim \mathcal{GP}(\boldsymbol{\mu}(t), \mathbf{K}(t, t')). \quad (3)$$

Moreover, this paper approximates the continuous collision-check model via up-sampling [2] between the conjugate support waypoints. And the random up-sampling helps generate the stochastic gradient (SG) detailed in Section III-C.1.

III. METHODOLOGY

In this paper, we first propose the overall frame of incrementally stochastic and accelerated gradient information mixed for trajectory optimization (iSAGO, Section III-A), where the whole collision-free motion planning consists of a finite number of sub-trajectory optimization with the penalty method. Moreover, we restart the AGD with Lipschitz constant reestimation (\mathcal{L} -reAGD, Section III-B) to elevate the convergence rate of convex optimization. Besides that, we propose STOMA in Section III-C to drag the trajectory out of the body-obstacle stuck case.

A. incrementally Stochastic and Accelerated Gradient information mixed for trajectory Optimization

Given the initial and goal waypoints, we interpolate the support waypoints between them via the GP-based Bayesian inference and gain an initial trajectory. Then iSAGO finds a series of collision-free waypoints meeting both the convex and non-convex cases where the initial trajectory gets stuck in obstacles, leading the OMP into local minima.

Considering the above cases, iSAGO (Algorithm 1, Figure 1) mixes the accelerated and stochastic gradient information. \mathcal{L} -reAGD (Section III-B) aims to solve the first case, while STOMA (Section III-C) tends to drag the trajectory into a convex sub-space. Moreover, iSAGO nests the above methods in *PenIter* (i.e., penalty method [25]) to meet the constraints like collision-free and motion constraints.

The above method is still SAGO optimizing the whole trajectory with mixed steps. However, it is inefficient because the whole trajectory consists of collision-free, in-collision, and in-stuck parts and the different part requires different

Algorithm 1: iSAGO

Input: initial local trajectory $\boldsymbol{\theta}_0$, initial \mathcal{GP} covariance \mathbf{K}_0 and cost functional $\mathcal{F}[\boldsymbol{\theta}_0]$.
Initialization: Set the initial tradeoff coefficient ρ , and build up an informed Bayesian tree.
for *reTrajIter* : $i = 1 \dots N_{uf}$ **do**
 Get noisy set $\Theta_{\mathfrak{N}} = \bigcup_{j=1}^{N_{\mathfrak{N}}} \boldsymbol{\theta}_{\mathfrak{N}}^j$ via (4);
 for $j = 1, \dots, N_{\mathfrak{N}}$ **do**
 Get initial sub-trajectory $\boldsymbol{\theta}_0 \leftarrow \boldsymbol{\theta}_{\mathfrak{N}}^j$ and its covariance matrix \mathbf{K}_0 in \mathcal{GP} ;
 for *PenIter* : $1 \dots N_{\rho}$ **do**
 Check the body-obstacle stuck according to Section III-C.1;
 if *isStuck* **then**
 Optimize $\boldsymbol{\theta}_0$ via Algorithm 3;
 else
 Optimize $\boldsymbol{\theta}_0$ via Algorithm 2;
 end
 if $\mathcal{F}_{iObs}(\boldsymbol{\theta}) < obstol$ **then**
 break
 else
 $\rho \leftarrow \kappa_c \cdot \rho$;
 end
 end
 Update the factors of Bayesian tree;
 end
end

methods. So we adopt the basic idea of iSAM2 [5] and build a Bayesian tree (BT) consisted of serial conjoint factors informed by the sub-functional of each support waypoint. Under the assumption that there is no significant factor in an optimal BT, we find out significant factors in *reTrajIter* nesting *PenIter* and optimize them incrementally (iSAGO). The mean value and standard deviation are computed by:

$$\mu_{\mathcal{F}} = \sum_{i=1}^N w_i \mathcal{F}(\theta_i), \quad \mathcal{D}_{\mathcal{F}} = \sqrt{\|\mathcal{F}(\boldsymbol{\theta}) - \mu_{\mathcal{F}}\|_{\mathbf{W}}^2}, \quad (4)$$

where $\mathbf{W} = \text{diag}(w_i)$ and $w_i = 1/N$. After estimating the mean $\mu_{\mathcal{F}}$ and deviation $\mathcal{D}_{\mathcal{F}}$, iSAGO gains a set of waypoints $\Theta_{\mathfrak{N}} = \{\theta_i \mid \|\mathcal{F}(\theta_i) - \mu_{\mathcal{F}}\| > \mathcal{D}_{\mathcal{F}}\}$ with significant factor. Then it regroups $\Theta_{\mathfrak{N}}$ into $\Theta_{\mathfrak{N}} = \bigcup_{j=1}^{N_{\mathfrak{N}}} \boldsymbol{\theta}_{\mathfrak{N}}^j$ whose elements $\theta_i \in \boldsymbol{\theta}_{\mathfrak{N}}^j$ are adjacent. Algorithm 1 and Figure 1 show how iSAGO optimizes every $\boldsymbol{\theta}_{\mathfrak{N}}^j$ by mixed steps generated by \mathcal{L} -reAGD and STOMA in *reTrajIter*. When $\Theta_{\mathfrak{N}}$ optimized, iSAGO updates the Bayesian tree, regenerates $\Theta_{\mathfrak{N}}^{j+1}$, and optimizes it incrementally. Note that κ_c updates ρ coincided with the sub-trajectory than the whole trajectory.

B. \mathcal{L} -restarted AGD for Trajectory Optimization

This paper introduces AGD to accelerate the nonlinear programming (NLP) when the initial trajectory is in a convex sub-space (i.e., not in-stuck). The traditional AGD methods [9], [10], [26] usually use a sustainable \mathcal{L} value for

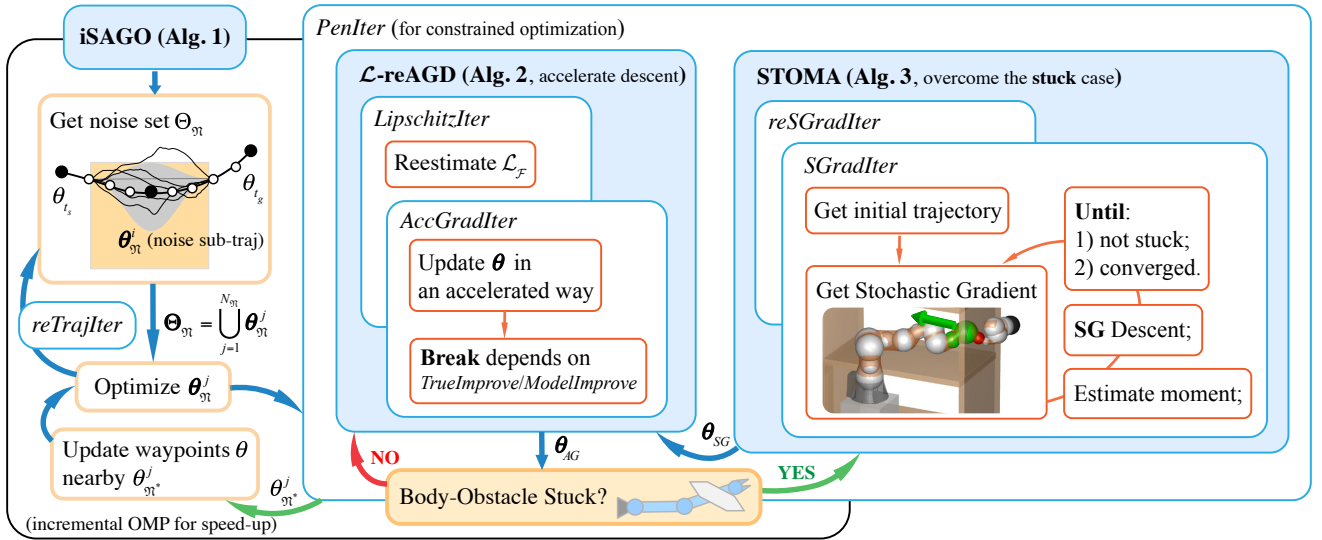


Fig. 1: A block diagram illustrates iSAGO (Algorithm 1, Section III-A) does collision-free OMP, whose outer layer shows how to refine a whole trajectory via BTI-based sub-trajectories optimization. The *PenIter* integrates \mathcal{L} -reAGD (Algorithm 2, Section III-B) and STOMA (Algorithm 3, Section III-C) to solve the non-convex OMP by detecting the stuck case.

the calculation of AGD steps. Though AGD free of the multi-estimation of step size is sometimes more efficient than the line search method, its convergence rate strongly relies on the initial \mathcal{L}_0 . Because a large or small \mathcal{L} -value may lead to a low or fluctuated descent process. In this way, we adopt the basic idea of sequential convex optimization [27] and propose \mathcal{L} -reAGD (Algorithm 2) nesting AGD (i.e., *AccGradIter*) in \mathcal{L} -restart process (i.e., *LipschitzIter*).

Algorithm 2: \mathcal{L} -reAGD

Input : Initial trajectory θ_0 , functional cost $\mathcal{F}(\theta_0)$, GP kernel \mathcal{K} and penalty factor ϱ .

Initialization: Set the initial Lipschitz constant $\mathcal{L}_{\mathcal{F}}$.

for *LipschitzIter* : $j = 1 \dots N_{\mathcal{L}}$ **do**

Reestimate $\mathcal{L}_{\mathcal{F}}$ and reinitialize $\{\theta_0, \theta_0^{md}, \theta_0^{ag}\}$;

for *AccGradIter* : $k = 1 \dots N_{ag}$ **do**

$\theta_k^{md} = (1 - \alpha_k) \theta_{k-1}^{ag} + \alpha_k \theta_{k-1}$;

Compute the functional gradient $\bar{\nabla} \mathcal{F}(\theta_k^{md})$;

Update α_k, β_k and λ_k by (6);

$\theta_k = \theta_{k-1} - \lambda_k \bar{\nabla} \mathcal{F}(\theta_k^{md})$;

$\theta_k^{ag} = \theta_k^{md} - \beta_k \bar{\nabla} \mathcal{F}(\theta_k^{md})$;

if converged to \mathcal{F}_{tol} **or** θ_{tol} **or** isStuck **then**

return θ_k^{md} .

end

if *pred/ared* $\notin (c_l, c_u)$ **then**

Reject $\{\theta_k, \theta_k^{md}, \theta_k^{ag}\}$;

break

end

end

As \mathcal{L} -reAGD is designed for NLP, we assume that \mathcal{F} is continuously differentiate and satisfies $\|\bar{\nabla} \mathcal{F}(\theta_y) -$

$$\bar{\nabla} \mathcal{F}(\theta_x)\| \leq \mathcal{L}_{\mathcal{F}} \|\theta_y - \theta_x\| \text{ when } \forall \theta_x, \theta_y \in \mathcal{C}_{\theta}:$$

$$\mathcal{C}_{\theta} = \{\theta' \mid |\mathcal{F}(\theta') - \mathcal{F}(\theta) - \langle \bar{\nabla} \mathcal{F}(\theta), \theta' - \theta \rangle| \leq \frac{\mathcal{L}_{\mathcal{F}}}{2} \|\theta' - \theta\|^2\}. \quad (5)$$

For the whole AGD process is a linear combination of descent step with different step size, we adopt the $\{\alpha_k, \beta_k, \lambda_k\}$ update rules in [10]:

$$\alpha_k = \frac{2}{k+1}, \quad \beta_k = \frac{1}{2\mathcal{L}_{\mathcal{F}}}, \quad \lambda_k = \frac{k\beta_k}{2}, \quad (6)$$

then for $\forall N > 1$, we have:

$$\min_{k=1 \dots N} \|\bar{\nabla} \mathcal{F}(\theta^{md})\|^2 \leq \frac{96\mathcal{L}_{\mathcal{F}} \|\theta^* - \theta_0\|^2}{N_{ag}^2 (N_{ag} + 1)}. \quad (7)$$

And we gain the time complexity $\mathcal{O}(\mathcal{L}_{\mathcal{F}}^{\frac{2}{3}}/\epsilon_{\theta}^{\frac{2}{3}})$ where $\|\bar{\nabla} \mathcal{F}\| \leq \epsilon_{\theta}$. So it is essential for the former AGD methods to make an optimal estimation of the initial $\mathcal{L}_{\mathcal{F}0}$. However, it is usually hard to decide a proper value when the NLP is not strongly convex. In this way, we reestimate $\mathcal{L}_{\mathcal{F}}$ and restart AGD process when the descent is too conservative or aggressive in the local convex hull (5).

Some prior studies like ODE-AG [11] and AR-AG [28] introduce the restart schemes for speeding up the convergence rate. This section first uses $\delta_0 \|\bar{\nabla}_{\hat{\theta}} \mathcal{F}(\hat{\theta})\|$ as $\mathcal{L}_{\mathcal{F}0}$, where δ_0 denotes the initial step-size. Then we adopt the fundamental thought in trust-region method [8] and propose an initial Lipschitz constant recalculation mixed with arbitrary expanding method. Our method exponentially expands $\mathcal{L}_{\mathcal{F}}$ with factor $\tau_{\mathcal{L}}$ when the step with current $\mathcal{L}_{\mathcal{F}}$ is rejected (i.e. *pred/ared* $\notin (c_l, c_u)$) in AGD initially, while recalculate $\mathcal{L}_{\mathcal{F}}$ otherwise. Based on (5), we define *pred* with $\delta_k^{md} = \theta_k^{md} - \theta_{k-1}^{md}$ as:

$$pred = \langle \bar{\nabla} \mathcal{F}(\theta_k^{md}), \delta_k^{md} \rangle + \frac{\mathcal{L}_{\mathcal{F}}}{2} \|\delta_k^{md}\|^2. \quad (8)$$

The above AGD restarted with reestimated $\mathcal{L}_{\mathcal{F}}$ could not only guarantee a fast descent with fewer times of step-size estimation but also a robust convergence.

C. Stochastic Optimization with Moment Adaptation

Some studies of deep learning [29] propose SGD methods for learning object with noisy or sparse gradients. Adam [14] optimizes the objective function consisted of sub-functions in low coupling. For the high robustness of Adam even facing the function variation compared to AdaGrad [30] and RMSProp [15], we adopt its moment adaptation method and propose STOMA (Algorithm 3, Figure 2) in the stuck case. This section will first illustrate how to detect the stuck case, generate the stochastic gradient (SG), and introduce how the SGD accelerated with moment adaptation.

Algorithm 3: STOMA

Input: Start and end states $\theta(t_0)$, $\theta(t')$, a state-dependent cost functional $\mathcal{F}[\theta_k(t)]$

- 1 **Initialization:** Mean value μ , covariance matrix \mathcal{K} .
- 2 **for** *reSGradIter*: $j = 1 \dots N_{rsg}$ **do**
- 3 Sample trajectories
 $\Theta = \{\theta_1, \dots, \theta_K | \theta_k \sim \mathcal{GP}(\mu, \mathcal{K})\};$
- 4 Evaluate trajectory costs $\{\mathcal{F}[\theta_1], \dots, \mathcal{F}[\theta_K]\};$
- 5 Take M samples with lowest cost from Θ ;
- 6 Reinitialize trajectory: $\theta_0 = \frac{\sum_{m=1}^M [p_m \theta_m(t)]}{\sum_{m=1}^M p_m};$
- 7 **for** *SGradIter*: $k = 1 \dots N_{sg}$ **do**
- 8 Update $N_{sg} \sim \mathcal{U}(N_{lo}^{sg}, N_{up}^{sg})$ randomly;
- 9 $\theta_k^{sg} = (1 - \alpha_k) \theta_{k-1}^{sg} + \alpha_k \theta_{k-1}$;
- 10 Compute the functional gradient $\bar{\nabla} \mathcal{F}(\theta_k^{sg})$
and check the body-obstacle stuck case;
- 11 **if not isStuck then**
- 12 **return** the optimum θ^{sg} .
- 13 **end**
- 14 **if** $\|\theta_k - \theta_{k-1}\| \leq SGtol$ **then**
- 15 Accept θ_k^{sg} via $\mu = \theta_k^{sg}$.
- 16 **break**
- 17 **end**
- 18 Estimate the 2^{nd} moment \mathfrak{M}_k via (13);
- 19 Update α_k , β_k and λ_k via (14);
- 20 $\theta_k = \theta_{k-1} - \lambda_k \bar{\nabla} \mathcal{F}(\theta_k^{sg})$;
- 21 $\theta_k^{ag} = \theta_k - \beta_k \bar{\nabla} \mathcal{F}(\theta_k^{sg})$;
- 22 **end**
- 23 **end**

1) Stuck case check and stochastic gradient generation:

According to the collision field shown in CHOMP [1], the obstacle cost functional is a finite accumulation of sub-functions calculated by the individual collision-check box (CCB) in discrete time. So we generate the SG in functional, time, and space during SGD. In the functional part, we gain $\bar{\nabla} \mathcal{F}^{sg}$ via $\varrho' \sim \mathcal{U}(\varrho, \infty)$. In the time part, we gain $\bar{\nabla} \mathcal{F}_{obs}^{sg}$ via $\{n_t^{ip}, \dots, n_{t_i}^{ip}, \dots, n_{t'-1}^{ip} | n_{t_i}^{ip} \sim \mathcal{U}(0, N^{ip})\}$ of interval time points between θ_{t_i} and $\theta_{t_{i+1}}$ in $[t, t']$,

$$\bar{\nabla} \mathcal{F}_{obs}^{sg} = \mathbf{M}_{sg}^\top \cdot \mathbf{g}_{up}, \quad (9)$$

where $\Lambda_{t_i}^{sg} = [\Lambda_{i,1}^\top \dots \Lambda_{i,n_{t_i}^{ip}}^\top]^\top$, $\Psi_{t_i}^{sg} = [\Psi_{i,1}^\top \dots \Psi_{i,n_{t_i}^{ip}}^\top]^\top$ are gained from Section II-A and [2],

$$\mathbf{M}_{sg} = \begin{bmatrix} \mathbf{I} & \mathbf{0} & \mathbf{0} & \dots & \dots & \dots & \mathbf{0} & \mathbf{0} \\ \Lambda_{t_i}^{sg} & \Psi_{t_i}^{sg} & \mathbf{0} & \dots & \dots & \dots & \mathbf{0} & \mathbf{0} \\ \vdots & \vdots & \ddots & & & & \vdots & \vdots \\ \mathbf{0} & \mathbf{0} & \dots & \mathbf{I} & \mathbf{0} & \dots & \mathbf{0} & \mathbf{0} \\ \mathbf{0} & \mathbf{0} & \dots & \Lambda_{t_i}^{sg} & \Psi_{t_i}^{sg} & \dots & \mathbf{0} & \mathbf{0} \\ \mathbf{0} & \mathbf{0} & \dots & \mathbf{0} & \mathbf{I} & \dots & \mathbf{0} & \mathbf{0} \\ \vdots & \vdots & & & & \ddots & \vdots & \vdots \\ \mathbf{0} & \mathbf{0} & \dots & \dots & \dots & \dots & \Lambda_{t'-1}^{sg} & \Psi_{t'-1}^{sg} \\ \mathbf{0} & \mathbf{0} & \dots & \dots & \dots & \dots & \mathbf{0} & \mathbf{I} \end{bmatrix} \quad (10)$$

maps the upsampled gradient

$$\mathbf{g}_{up} = \begin{bmatrix} \nabla^\top \mathcal{F}_{obs}^\mathbf{B}(\theta_t), \\ \nabla^\top \mathcal{F}_{obs}^\mathbf{B} \left[\theta \left(t + \frac{1}{n_t^{ip} + 1} \right) \right], \dots, \nabla^\top \mathcal{F}_{obs}^\mathbf{B}(\theta_{t+1}), \\ \dots, \\ \nabla^\top \mathcal{F}_{obs}^\mathbf{B} \left[\theta \left(t' - \frac{n_{t'-1}^{ip}}{n_{t'-1}^{ip} + 1} \right) \right], \dots, \nabla^\top \mathcal{F}_{obs}^\mathbf{B}(\theta_{t'}) \end{bmatrix}^\top \quad (11)$$

into the gradient $\bar{\nabla} \mathcal{F}_{obs}^{sg}$ of the support waypoints $\theta_{t,t'}$.

Different from the above rules in functional and time, the intuition of SG-rule in space comes from the collision avoidance of the human arm in a narrow workspace, such as a bookshelf shown in Figure 3. When a blindfolded participant stretches across the bookshelf for an object, he makes reflexes alternatively in response to the arm-obstacle collision. The arm parts in danger, denoted by orange/red balls, stimulate the reflexes via the exterior forces denoted by the orange arrows.

Figure 4 demonstrates a tandem manipulator composed of rigid bodies coupled in series, each of which is geometrically reconstructed by the CCBs related to the balls in Figure 3. The obstacle avoidance trajectory (black curve) of the human arm indicates the collision risk rises from shoulder to hand. In this way, we build each sub-problem (i.e., the local collision avoidance) from shoulder to end-effector (EE). And $\bar{\nabla} \mathcal{F}_{obs}$ is calculated via the accumulation of CCB-gradients from \mathcal{B}_1 close to shoulder up to \mathcal{B}_k close to EE:

$$\nabla \mathcal{F}_{obs}^k = \sum_{\substack{\mathcal{B}_i \in \mathbf{B}_k, \\ \phi_i < \phi_{tol}}} \nabla_{q_i} \mathcal{F}_{obs}, \quad \mathbf{B}_k = \{\mathcal{B}_1, \dots, \mathcal{B}_k\}, \quad (12)$$

where q_i contains joints $\{\theta^d\}$ actuating CBB- \mathcal{B}_i in workspace, and ϕ_i is the included angle between \mathcal{B}_i -gradient $\nabla_{q_i} \mathcal{F}_{obs}$ and the accumulated gradient $\nabla \mathcal{F}_{obs}^{i-1}$ (from \mathcal{B}_1 to \mathcal{B}_{i-1}). When there exists a $\phi_i > \phi_{tol}$, we think the waypoint θ_{t_i} stuck in an obstacle. In this way, the random ϕ_{tol} generates SG, where we reject $\nabla_{q_k} \mathcal{F}_{obs}$ when $\phi_k > \phi_{tol}$.

2) *Update rules:* Adam [14] adopts the piecewise production of gradients and uses EMA from the initial step up to the current step and the bias correction method for the adaptive moment estimation. In our work, we make the squared ℓ_2 -norm of functional gradient $\bar{\nabla}_\theta \mathcal{F}$, and also adopts EMA and bias correction technology for $\{\mathfrak{M}_k\}$ estimation:

$$\hat{\mathfrak{M}}_k = \gamma \hat{\mathfrak{M}}_{k-1} + (1 - \gamma) \bar{\nabla} \mathcal{F}(\theta_k^{sg})^{\odot 2}, \quad \mathfrak{M}_k = \frac{\hat{\mathfrak{M}}_k}{1 - \gamma^k}. \quad (13)$$

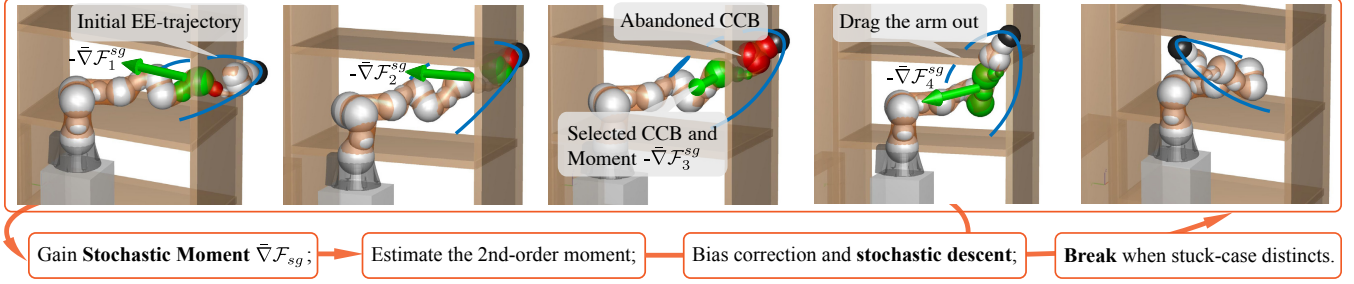


Fig. 2: An example shows how STOMA (Algorithm 3, Section III-C) drags the manipulator out of the body-obstacle situation via stochastic gradient descent with adaptive moment estimation. Note that the green CCBs are selected for SG (i.e., 1st moment, denoted by green arrow) generation while the red ones are abandoned.



Fig. 3: A series of frames illustrate how the human arm reacts to obstacles when grasping inside a bookshelf. The green, orange, and red balls show the none, low and high-risk areas of collision, respectively.

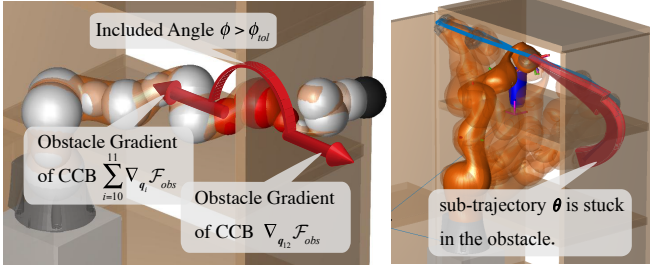


Fig. 4: An assembly of grey boxes presents an LBR-iiwa for collision check, and the red box denotes the collision case. The stuck case happens when the included angle $\phi > \phi_{tol}$.

As shown in Algorithm 3, we adopt the AGD rules [10] than bias correction combined EMA method for 1st moment adaption. And the parameters $\{\alpha_k, \beta_k, \lambda_k\}$ update as

$$\alpha_k = \frac{2}{k+1}, \quad \beta_k = \frac{1}{2\delta\sqrt{m_k}}, \quad \lambda_k \in \left[1, 1 + \frac{\alpha_k}{4}\right]. \quad (14)$$

In this way, the descent process approximately bounded by a δ -sized trust region accelerates via the α -linear interpretation between the conservative step and the accelerated step driven by $\{\lambda_k\}$ and $\{\beta_k\}$ correspondingly. Then the process varies from the lag state guided by θ to the shifting one guided by θ^{ag} with $\{\alpha_k\}$ value. Considering the SGD is roughly under $\mathcal{L}_{\mathcal{F}}\text{-}\mathcal{C}_{\theta^{sg}}$ mentioned in (5), we get

$$\begin{aligned} \mathcal{F}_{k-1} &\leq \mathcal{F}_k + \langle \bar{\nabla} \mathcal{F}_{k-1}, \theta_k - \theta_{k-1} \rangle \\ &\leq \mathcal{F}_k + \lambda_k \|\bar{\nabla} \mathcal{F}_k^{sg}\|^2 + \lambda_k \|\Delta_k\| \|\bar{\nabla} \mathcal{F}_k^{sg}\|, \end{aligned} \quad (15)$$

where $\mathcal{F}_k, \mathcal{F}_k^{sg}$ are the abbreviations of $\mathcal{F}(\theta_k), \mathcal{F}(\theta_k^{sg})$, and $\|\Delta_k\| = \|\bar{\nabla} \mathcal{F}_{k-1} - \bar{\nabla} \mathcal{F}_k^{sg}\| \leq \mathcal{L}_{\mathcal{F}}(1 - \alpha_k)\|\theta_{k-1}^{ag} - \theta_{k-1}\|$. Considering $\theta_k^{ag} - \theta_k = (1 - \alpha_k)(\theta_{k-1}^{ag} - \theta_{k-1}) + (\lambda_k - \beta_k)\bar{\nabla} \mathcal{F}_k^{sg}$ based on Algorithm 3 (line 9, 10, 22) and Cauchy-Schwarz inequation, we get

$$\begin{aligned} \mathcal{F}_{k-1} &\leq \mathcal{F}_k + \lambda_k(1 + \mathcal{L}_{\mathcal{F}}\lambda_k/2)\|\bar{\nabla} \mathcal{F}_k^{sg}\|^2 \\ &\quad + \mathcal{L}_{\mathcal{F}}(1 - \alpha_k)^2\|\theta_{k-1}^{ag} - \theta_{k-1}\|^2/2. \end{aligned} \quad (16)$$

Then through the accumulation from $k = 1$ to N_{sg} , we get

$$\frac{\mathcal{F}_0 - \mathcal{F}_{N_{sg}}}{\mathcal{L}_{\mathcal{F}}} \leq \sum_{k=1}^{N_{sg}} \left(\lambda_k + \frac{\lambda_k^2}{2} + \frac{(\lambda_k - \beta_k)^2}{2\Gamma_k\alpha_k} \sum_{\tau=k}^{N_{sg}} \Gamma_{\tau} \right) \|\bar{\nabla} \mathcal{F}_k^{sg}\|^2, \quad (17)$$

where $\Gamma_k = (1 - \alpha_k)\Gamma_{k-1}$ with $\Gamma_0 = 1$. In sight of the stochasticity of functional $\mathcal{F}(\theta^{sg})$ and its gradient $\bar{\nabla} \mathcal{F}(\theta^{sg})$ and presuming that $\|\bar{\nabla} \mathcal{F}_k\|_{c_l} \cdot \delta \geq \mathcal{L}_{\mathcal{F}}$, we get:

$$\frac{\mathcal{F}_0 - \mathcal{F}_{N_{sg}}}{N_{sg}} \leq \frac{5G_{\infty}}{4\delta} \left(1 + \frac{11c_l}{32} \right) \frac{\ln(N_{sg} + 1)}{N_{sg}}, \quad (18)$$

where c_l is the fraction of $\mathcal{L}_{\mathcal{F}}$ and trust region box, $G_{\infty} \leq \mathbb{E}(\|\bar{\nabla}^T \mathcal{F}_1, \dots, \bar{\nabla}^T \mathcal{F}_{N_{sg}}\|_{\infty})$.

Figure 2 illustrates how the manipulator reflexes to the stuck case following the update rules in *SGradIter*. To improve the computational efficiency and success rate, we nest the above process (i.e., *SGradIter*) in *reSGradIter*, where we generate the initial trajectory $\theta_0 = \mu$ via the expectation calculation of M low-cost samples in K samples. And we get the maximum number of *SGradIter* randomly in $[N_{lo}^{sg}, N_{up}^{sg}]$.

IV. EXPERIMENT

This section will first introduce how to construct the objective functional in Section IV-A. Then it will detail the benchmark and parameter setting in Section IV-B.1 and Section IV-B.2, and analysis the benchmark results in Section IV-B.3. Finally, it will demonstrate how iSAGO implements in an AUBO-i5 robot with 6 DoFs.

A. Implementation details

1) *GP prior*: To decrease the dimension of configuration/state space, we assume the joint velocity is constant and gain the LTV-SDE as well as the GP prior [2]. Moreover, our benchmark sets 12 support states with 8 intervals (116 states in total) for iSAGO and GPMP2, 116 states for STOMP and

CHOMP, 2 or 58 sates for TrajOpt, and MaxConnection-Distance = $\frac{\|\theta_g - \theta_0\|}{12}$ for RRT-Connect.

2) *Collision cost function*: Our work adopts the polynomial piecewise form [1] for the collision cost function.

3) *Motion constraints*: The motion cost function in GPMP [2] is adopted to drive the robot under the preplanned optimal collision-free trajectory in the real world.

B. Evaluation

1) *Setup for benchmark*: This paper benchmarks iSAGO against the numerical based motion planner: CHOMP [1], TrajOpt [7], GPMP2 [2], as well as the sampling-based motion planner: STOMP [17], RRT-Connect [31] in 7-DoF LBR-iiwa robot. For the benchmark executes in MATLAB, we install the compiled GPMP2-toolbox and use BatchTrajOptimize3DArm to implement GPMP2 [2] and use plannerBiRRT to implement RRT-Connect [31]. TrajOpt is an SCO with the trust-region method internally using Gurobi. So our benchmark uses fmincon with options = optimoptions('fmincon','Algorithm','trust-region-reflective','SpecifyObjectiveGradient',true), which calculates ObjectiveGradient analytically and Aeq (the matrix whose rows are the active constraint gradients) via numerical differentiation like TrajOpt. For CHOMP adopts the HMC method for optimal trajectory and its momentum, our benchmark defines an hmcSampler object whose logarithm probabilistic density function (logpdf) is defined as (2), uses hmcSampler.drawSamples for HMC, and compiles it in CMex-file. As for STOMP, our benchmark uses mvnrnd for noise trajectories sampling and updates the trajectory via projected weighted averaging [17].

To illustrate the competence of iSAGO for OMP problems, we conduct 25 experiments with different start or goal states in the same environment. We categorize the problems into 3 classes (A, B, and C, Figure 5) whose planning difficulty rises with the stuck cases in the initial trajectory increase. Considering the difficulty of different categories, we generate 2 tasks for class A, 3 for class B, and 4 for class C. Each task consists of several sub-problems with random initial or different goal configurations satisfying the goal constraint. Moreover, we compare iSAGO with SAGO to illustrate the computational efficiency of iOMP.

2) *Parameter setting*: As STOMA (Algorithm 3, Figure 2) proceeds SGD roughly contained in a δ -trust region with γ -EMA of historical moments, this section first introduces the key parameter tuning then the others.

According to abundant experiences, we tune the key parameters around $\{\delta = 1.25, \gamma = 0.1\}$. We conduct 10 different C-class tasks when tuning $\{\delta, \gamma\}$ and estimate the 95% confidence interval of the SGD's expectation. Each sub-figure of Figure 6 illustrates 10 SGDs and their confidence interval denoted by the purple area under a specific $\{\delta, \gamma\}$. The larger interval of $\delta = 1.25$ indicates the lower robustness of SGD, meaning the unstable iSAGO, while the higher SGD-rate of $\gamma = 0.99$ indicates the higher efficiency.

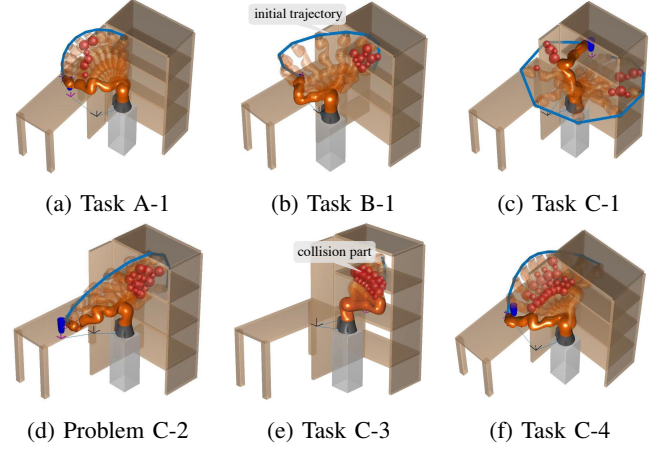


Fig. 5: A figure shows some of the experiments, where some body parts of sub-trajectories interfere with environment. Note that *Problem X1-X2* means task X2 in class X1.

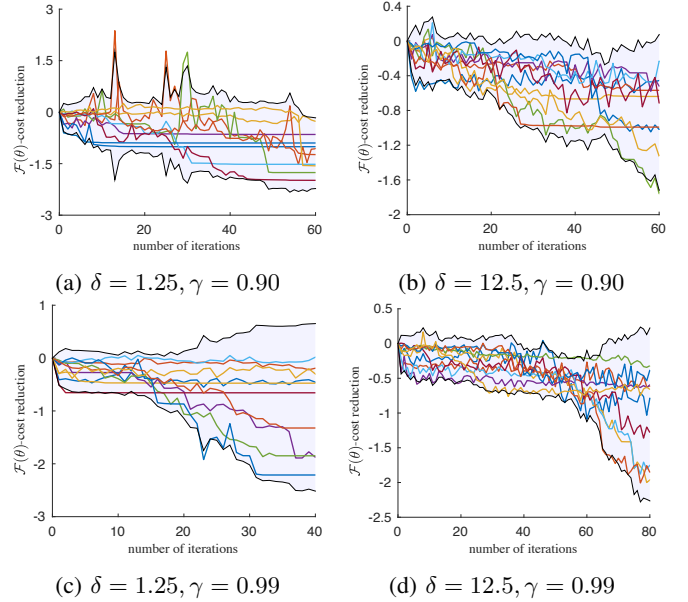


Fig. 6: A figure shows the result of δ, γ adjustment.

To further demonstrate the key parameter tuning, we make a statistic analysis of the results under variant $\{\delta \in [1.25, 25], \gamma \in [0.5, 0.99]\}$. Table I, where '(%)' and '(s)' denote success rate and average time, respectively, indicates the SGD-rate increases with δ -descent. In contrast, the success rate decreases with the excessive δ (i.e., too high or low). Moreover, the SGD-rate increases with γ -descent while the success rate decreases with γ -descent. In this way, we choose $\{\delta = 6.25, \gamma = 0.95\}$ as default parameters.

Besides δ and γ , we choose $Q_{C0} = I$ or $Q_{C0} = \text{diag}(5e-2, 1, 5e-2, 5e-2, 2.5e-2, 5e-2, 1e-2)$. In Algorithm 1, we set the initial penalty $\varrho = 1.25e-2$ and penalty factor $\tau_c = 0.4$. In Algorithm 2, we set the threshold or tolerance $c_l = 0.1$, $c_u = 0.9$, $\mathcal{F}tol = 8e-4$, $\theta tol = 10^{-3}$, and the arbitrary Lipschitz factor $\tau_L = 6.67$. In Algorithm 3, we set the number of samples and the selected samples as

TABLE I: Results for $\{\delta, \gamma\}$ tuning of 10 tasks in class C

$(\%) \mid (s) \searrow \delta$ γ	1.25	6.25	12.5	25
0.5	80 1.253	90 1.898	70 4.198	40 6.309
0.9	90 2.512	100 2.463	80 4.973	60 8.219
0.99	90 2.672	100 3.089	80 7.131	60 12.57

$K = 12$ and $M = 6$ respectively, tolerance $SGtol = 6.4e-3$, $ImpRtol = 0$, and generate $N_{sg} \sim \mathcal{U}(35, 55)$. Note that we select $\phi_{tol} = 95^\circ$ for stuck case check and generate SG by selecting $\phi_{tol} \sim \mathcal{U}(60^\circ, 180^\circ)$. Moreover, we choose $\epsilon = 0.1$ for collision check and $\epsilon = 0.01$ for motion constraint.

3) *Results analysis*: The successful OMPs in Figure 7 guide the iiwa arm to actuate safely with high smoothness in the narrow workspace. Moreover, Class C's benchmark results in Table II illustrate iSAGO gains the highest success rate (Scr) compared to the others. The random SGradIter number and \mathcal{L} -reAGD help iSAGO gain the forth solving rate after TrajOpt-12, TrajOpt-58, and GPMP2-12. Though TrajOpt-58 compensates for the time-continuous safety information leak in TrajOpt-12, it still cannot escape from the local minima arising from SCO (trust-region) and gains the second lowest Scr just above TrajOpt-12. However, iSAGO successfully descends into the optimum informed by SG and its adaptive moment with a proper initial trust region. Thanks to HMC, gaining the Hamiltonian momentum randomly, CHOMP approaches the optimum with the third-highest Scr, whose failures are informed by the exact moment than the adaptive stochastic moment. RRT-Connect has the second-highest Scr regardless of the largest computational source for RRT growing restricted by MaxConnectionDistance, negatively affecting Scr. Though STOMP is free of gradient calculation, the significant times it takes to resample do a minor effect for feasible searching, mainly limited by the Gaussian covariance. As for GPMP2-12 and TrajOpt-58, LM and trust-region method help them approach the stationary point rapidly, while whether the point is feasible highly depends on the initial value. Furthermore, the comparison between iSAGO and SAGO indicates a higher efficiency, roughly 30%, of BTI-based incremental planning.

4) *Industrial Implementation*: This part will illustrate how an AUBO-i5 robot with 6 DoFs makes collision-free planning to grab and load a pack of Mi-speaker in a storage shelf whose high compact structure ensures a high storage volume. The red area on initial trajectories of the tasks in Figure 8 shows the interference between the arm and the shelf when AUBO-i5 is transferring the pack between different cells. In this way, our implementation sets $Q_{C0} = \text{diag}(5e-2, 1, 5e-2, 5e-2, 2.5e-2, 5e-2, 1e-2)$ for GP prior, $\epsilon = 0.025$ for collision-check considering the narrow space of the shelf, and the others following Section IV-B.2. To further test iSAGO's solvability, we conduct 5 repeated trials for each task given an initial state and goal constraint. Figure 8b shows that AUBO-i5 grabs the Mi-pack in a cell of the shelf from the default state, and Figure 8d shows it loads the pack from one cell to another, bypassing the laminate and support

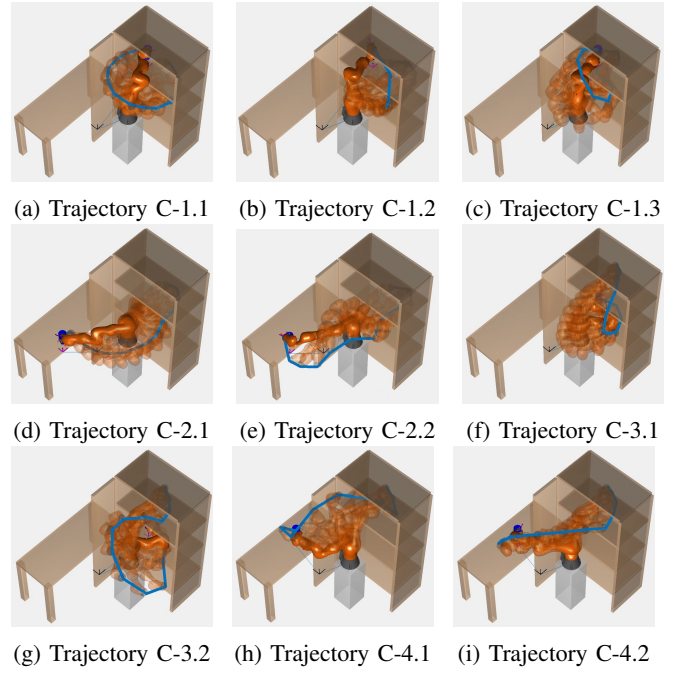


Fig. 7: A figure shows some results of iSAGO in class C. Note that $X3$ in Trajectory $X1$ - $X2$. $X3$ means a single problem $X3$ in task $X2$ categorized into class $X1$.

arms of the shelf. The 100% Scr with 2.143s average time shows the high reliability and efficiency of iSAGO.

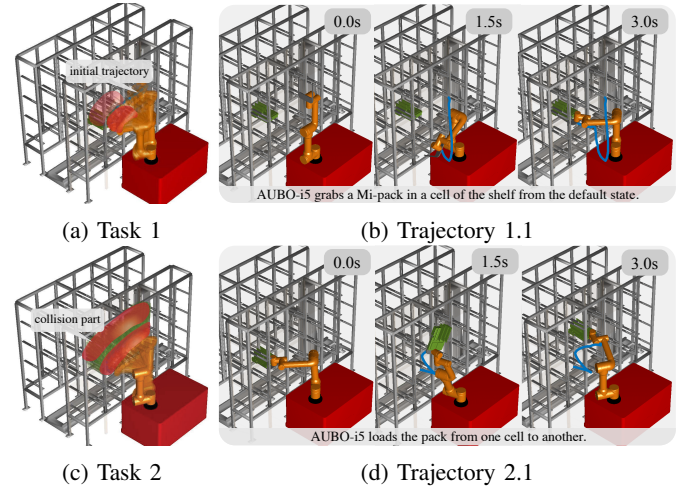


Fig. 8: An AUBO-i5 grabs/loads a Mi-pack in a storage shelf.

V. CONCLUSIONS

iSAGO utilizes the mixed information of accelerated (\mathcal{L} -reAGD) and stochastic (STOMA) moments on the penalty method to overcome the body-obstacle stuck cases in the narrow workspace. The benchmark results show that 1) STOMA improve the success rate by 2.1 to 24 times compared to the numerical OMP and 20% to 275% compared to the sampling OMP in the limited time. 2) The BTI-based incremental

TABLE II: Results for 16 planning problems in class C

	SAGO	iSAGO	TrajOpt-12	TrajOpt-58	GPMP2-12	CHOMP	STOMP	RRT-Connect
Suc. Rate (%)	91.25	93.75	3.75	8.75	11.25	30	25	72.5
Avg. Time (s)	4.284	2.132	0.232	1.108	2.464	6.989	7.691	13.65
Std-Dev. Time (s)	1.048	0.319	0.055	0.101	1.312	1.290	5.233	4.562
Max. Time (s)	6.981	3.753	0.348	1.583	5.091	9.534	17.16	20.64

planning (iSAGO) helps improve the efficiency of SAGO by 22%. Moreover, **3)** \mathcal{L} -reAGD helps iSAGO take 64% to 81% less computational time than the sampling OMP and only takes some extra time (0.2s to 2.1s) compared to the numerical OMP.

ACKNOWLEDGMENT

The work of this paper is partially supported by the National Key R&D Program of China (No.2017YFB1301203), the National Natural Science Foundation of China (No. 51675470 & 51805531), the Key R&D Program of Zhejiang Province (2020C01025, 2020C01026), and Robotics Institute of Zhejiang University Grant (K11808).

References

- [1] M. Zucker, N. Ratliff, A. D. Dragan, M. Pivtoraiko, M. Klingensmith, C. M. Dellin, J. A. Bagnell, and S. S. Srinivasa, "Chomp: Covariant hamiltonian optimization for motion planning," *The International Journal of Robotics Research*, vol. 32, no. 9-10, pp. 1164–1193, 2013.
- [2] M. Mukadam, J. Dong, X. Yan, F. Dellaert, and B. Boots, "Continuous-time gaussian process motion planning via probabilistic inference," *The International Journal of Robotics Research*, vol. 37, no. 11, pp. 1319–1340, 2018.
- [3] K. Shirley, "Inference from simulations and monitoring convergence," *Handbook of Markov Chain Monte Carlo*, May 2011.
- [4] M. Bhardwaj, B. Boots, and M. Mukadam, "Differentiable gaussian process motion planning," in *2020 IEEE International Conference on Robotics and Automation (ICRA)*, May 2020, pp. 10598–10604.
- [5] M. Kaess, H. Johannsson, R. Roberts, V. Ila, J. J. Leonard, and F. Dellaert, "isam2: Incremental smoothing and mapping using the bayes tree," *The International Journal of Robotics Research*, vol. 31, no. 2, pp. 216–235, 2012.
- [6] K. Levenberg, "A method for the solution of certain non-linear problems in least squares," *Quarterly of Applied Mathematics*, vol. 2, no. 2, pp. 164–168, 1944.
- [7] J. Schulman, J. Ho, A. X. Lee, I. Awwal, H. Bradlow, and P. Abbeel, "Finding locally optimal, collision-free trajectories with sequential convex optimization," in *Robotics: science and systems*, vol. 9, no. 1. Citeseer, 2013, pp. 1–10.
- [8] R. H. Byrd, J. C. Gilbert, and J. Nocedal, "A trust region method based on interior point techniques for nonlinear programming," *Mathematical programming*, vol. 89, no. 1, pp. 149–185, 2000.
- [9] Y. Nesterov, "A method for unconstrained convex minimization problem with the rate of convergence $O(1/k^2)$," in *Doklady an ussr*, vol. 269, 1983, pp. 543–547.
- [10] S. Ghadimi and G. Lan, "Accelerated gradient methods for nonconvex nonlinear and stochastic programming," *Mathematical Programming*, vol. 156, no. 1-2, pp. 59–99, 2016.
- [11] W. Su, S. Boyd, and E. Candes, "A differential equation for modeling nesterov's accelerated gradient method: Theory and insights," in *Advances in Neural Information Processing Systems 27*, Z. Ghahramani, M. Welling, C. Cortes, N. D. Lawrence, and K. Q. Weinberger, Eds. Curran Associates, Inc., 2014, pp. 2510–2518.
- [12] A. C. Wilson, B. Recht, and M. I. Jordan, "A lyapunov analysis of momentum methods in optimization," 2018.
- [13] L. Bottou, "Large-scale machine learning with stochastic gradient descent," in *Proceedings of COMPSTAT'2010*, Y. Lechevallier and G. Saporta, Eds. Heidelberg: Physica-Verlag HD, 2010, pp. 177–186.
- [14] D. P. Kingma and J. Ba, "Adam: A method for stochastic optimization," *arXiv preprint arXiv:1412.6980*, 2014.
- [15] H. Geoffrey, N. Srivastava, and K. Swersky, "Neural networks for machine learning lecture 6a overview of mini-batch gradient descent," Department of Computer Science, University of Toronto, Tech. Rep. 14, 02 2012.
- [16] X. Wu and M. W. Mueller, "In-flight range optimization of multi-copters using multivariable extremum seeking with adaptive step size," in *2020 IEEE/RSJ International Conference on Intelligent Robots and Systems (IROS)*, 2020, pp. 1545–1550.
- [17] M. Kalakrishnan, S. Chitta, E. Theodorou, P. Pastor, and S. Schaal, "Stomp: Stochastic trajectory optimization for motion planning," in *2011 IEEE International Conference on Robotics and Automation*, May 2011, pp. 4569–4574.
- [18] L. E. Kavraki, M. N. Kolountzakis, and J. . Latombe, "Analysis of probabilistic roadmaps for path planning," *IEEE Transactions on Robotics and Automation*, vol. 14, no. 1, pp. 166–171, Feb 1998.
- [19] S. Karaman and E. Frazzoli, "Sampling-based algorithms for optimal motion planning," *The international journal of robotics research*, vol. 30, no. 7, pp. 846–894, 2011.
- [20] K. Solovey, O. Salzman, and D. Halperin, "New perspective on sampling-based motion planning via random geometric graphs," *The International Journal of Robotics Research*, vol. 37, no. 10, pp. 1117–1133, 2018.
- [21] E. W. Dijkstra, "A note on two problems in connexion with graphs," *Numerische Mathematik*, vol. 1, no. 1, pp. 269–271, 1959.
- [22] A. G. Hofmann, E. Fernandez, J. Helbert, S. D. Smith, and B. C. Williams, "Reactive integrated motion planning and execution," in *Twenty-Fourth International Joint Conference on Artificial Intelligence*, 2015.
- [23] S. M. LaValle *et al.*, "Rapidly-exploring random trees: A new tool for path planning," 1998.
- [24] P. Rajendran, S. Thakar, A. M. Kabir, B. C. Shah, and S. K. Gupta, "Context-dependent search for generating paths for redundant manipulators in cluttered environments," in *2019 IEEE/RSJ International Conference on Intelligent Robots and Systems (IROS)*, 2019, pp. 5573–5579.
- [25] J. Nocedal and S. Wright, *Numerical optimization*. Springer Science & Business Media, 2006.
- [26] Y. Nesterov, *Introductory lectures on convex optimization: A basic course*. Springer Science & Business Media, 2013, vol. 87.
- [27] A. R. Conn, N. I. M. Gould, and P. L. Toint, *Trust-Region Methods*. USA: Society for Industrial and Applied Mathematics, 2000.
- [28] B. O'Donoghue and E. Candès, "Adaptive restart for accelerated gradient schemes," *Foundations of Computational Mathematics*, vol. 15, no. 3, pp. 715–732, 2015.
- [29] I. Goodfellow, Y. Bengio, and A. Courville, *Deep learning*. MIT press, 2016.
- [30] J. Duchi, E. Hazan, and Y. Singer, "Adaptive subgradient methods for online learning and stochastic optimization," *J. Mach. Learn. Res.*, vol. 12, pp. 2121–2159, Jul. 2011.
- [31] J. J. Kuffner and S. M. LaValle, "Rrt-connect: An efficient approach to single-query path planning," in *Proceedings 2000 ICRA. Millennium Conference. IEEE International Conference on Robotics and Automation. Symposia Proceedings (Cat. No.00CH37065)*, vol. 2, April 2000, pp. 995–1001 vol.2.